Available online at www.sciencedirect.com
ScienceDirect
Polymer 49 (2008) 1860–1870
polymer
www.elsevier.com/locate/polymer

Simultaneous reinforcing and toughening: New nanocomposites of waterborne polyurethane filled with low loading level of starch nanocrystals

Guangjun Chen [a], Ming Wei [a], Jinghua Chen [a], Jin Huang [a,b,*], Alain Dufresne [b], Peter R. Chang [c,**]

[a] College of Chemical Engineering, Wuhan University of Technology, Wuhan 430070, China
[b] Ecole Francaise de Papeterie et des Industries Graphiques, Institut National Polytechnique de Grenoble (EFPG-INPG) BP65, 38402 Saint-Martin d'Héres Cédex, France
[c] Bioproducts and Bioprocesses National Science Program, Agriculture and Agri-Food Canada, 107 Science Place, Saskatoon, SK S7N 0X2, Canada

Received 4 November 2007; received in revised form 5 February 2008; accepted 14 February 2008
Available online 16 February 2008

Abstract

New nanocomposites of waterborne polyurethane (WPU) as a matrix were prepared by filling low loading of starch nanocrystals (StNs) as a nano-phase. It is worth noting that the resultant StN/WPU nanocomposites showed significant enhancements in strength, elongation and Young's modulus. Herein, the key role of StN in simultaneous reinforcing and toughening was disclosed, namely active surface and rigidity facilitated forming the interface of transferring stress and contributed to enduring stress, respectively. The preserving of original structure and interaction in WPU matrix was also the essential guarantee of improving mechanical performances. As the StN loading increased, the self-aggregation of StNs caused size expansion of nano-phase along with the increase of number, and hence they decreased the mechanical performances. Furthermore, it was verified that chemical grafting onto the StN surface didn't favor enhancing the strength and elongation, due to inhibiting the formation of physical interaction and increasing network density in nanocomposites.

Keywords: Waterborne polyurethane; Starch nanocrystal; Nanocomposites

1. Introduction

Natural polymers from renewable resources show the advantages of biodegradability, biocompatibility, non-toxicity, high reactivity, low cost, easy-to-availability and so on, and hence they have been considered as excellent raw chemical substances for saving petroleum resources and protecting the environment [1–3]. Born out of the growing interest in the predominant properties attributed to nano-fillers in composites, a kind of novel nano-materials derived from natural polymers, named as ''green'' bionanocomposites [4], has been developed, in which natural polymers can act as the matrix, the nano-filler or both. Usually, natural nano-fillers are the crystalline residue with a uniform structure after acidic or alkaline hydrolysis of natural polysaccharides, and the alternatives are so-called rod-like whiskers of cellulose [5] and chitin [6], and platelet-like nanocrystal of starch [7,8]. They not only inherit all the advantages of natural polymers, but also show a reinforcing function in composites by virtue of their rigidity similar to those traditional inorganic nano-fillers [5,6,9–11]. Moreover, compared with inorganic nano-fillers, a relatively active surface of natural nano-fillers is easier to perform chemical derivation and grafting [12–14] or form

* Corresponding author. College of Chemical Engineering, Wuhan University of Technology, 122 Loushi Road, Wuhan, Hubei 430070, China. Tel.: +86 27 63373510; fax: +86 27 87859019.
** Corresponding author.
E-mail addresses: huangjin@iccas.ac.cn (J. Huang), changp@agr.gc.ca (P.R. Chang).

0032-3861/$ - see front matter © 2008 Elsevier Ltd. All rights reserved.
doi:10.1016/j.polymer.2008.02.020

strong physical interaction [5] as well as comparatively easy processability due to their non-abrasive nature and other resultant functional properties [5]. So far, the cellulose and chitin whiskers as well as starch nanocrystal have successfully reinforced many natural and synthetic materials, such as natural rubber [5,10,15], polypropylene [16,17], poly(vinyl chloride) [18], poly(vinyl acetate) [19], poly(ethylene-*co*-vinyl acetate) [20], poly(styrene-*co*-butyl acrylate) [21], waterborne epoxy [22,23], poly(oxyethylene) [24], waterborne polyurethane [25], poly(β-hydroxyoctanoate) [26,27], poly(lactic acid) [28,29], polycaprolactone [30], silk fibroin [31], cellulose acetate butyrate [32], starch [9,33] and soy protein [34–36] plastics. Especially, the starch nanocrystals hydrolyzed from starch granules can also show an excellent reinforcing function as nano-filler for starch plastics [9].

Due to the increasing concern about human health and environment-friendliness, organic solvent-free polyurethane (i.e. waterborne polyurethane) has been rapidly developed and applied due to low volatile organic compound (VOC) and non-toxicity [37,38]. To enhance biodegradability, natural polymers have been incorporated into waterborne polyurethane matrix by mechanically blending or interpenetrating polymer networks. The selective incorporation of starch [39], soy protein [40] and lignin [41] into the composites not only induces bacterial proliferation, but also improves mechanical performances and lowers the cost. At the same time, cellulose whisker as a reinforcing nano-phase has also been filled into waterborne polyurethane matrix, resulting in a significant increase of strength and Young's modulus [25]. To our knowledge, however, research on the other natural nano-filler, i.e. starch nanocrystal, for modifying waterborne polyurethane can hardly be found in the literature. The distinct platelet-like structure of starch nanocrystal as well as its rigidity, which is similar to the exfoliated layered silicate [42,43], is expected to produce extraordinary mechanical performances.

In this work, we incorporated starch nanocrystals (StNs), which were hydrolyzed from potato starch granules, into waterborne polyurethane (WPU) matrix at the given stage in a typical process of synthesizing WPU, such as mixing with WPU latex post of emulsification (Method I), in the midst of emulsification (Method II) and chain-extending of polyurethane prepolymer (Method III). Subsequently, the structure and mechanical properties of resultant nanocomposite materials were investigated by attenuated total reflection-Fourier transform infrared spectroscopy (ATR-FTIR), X-ray diffraction (XRD), differential scanning calorimetry (DSC), dynamic mechanical analysis (DMA), scanning electron microscope (SEM) and tensile tests. Because the number of residual active isocyanate groups are determined by the selected three stages of adding StNs, the effects of chemical grafting and physical interaction, associated with active −OH onto the StN surface, on mechanical properties were discussed. Different from the previous reports of filling high content of whisker and nanocrystal into polymer matrix to simply increase strength and modulus, the low loading level of StNs still enhanced the elongation at one time in this work. As a result, the mechanism of simultaneous reinforcing and toughening was explored.

2. Experimental part

2.1. Materials

Potato starch was purchased from Sinopharm Chemical Reagent Co. Ltd. (Shanghai, China), and used as-received. Poly(1,4-butylene glycol adipate) with a number-average molecular weight (M_n) of 2000 (PBA_{2000}) and dimethylol propionic acid (DMPA) were, respectively, donated by Nanjing Zhongshan Co. Ltd. (Jiangsu, China) and Huzhou Changsheng Co. Ltd. (Zhejiang, China), and dehydrated under vacuum at 60 °C for 12 h. Toluene diisocyanate (TDI) and triethylamine (TEA) were purchased from Sinopharm Chemical Reagent Co. Ltd. (Shanghai, China), and redistilled before use. Butanone of analytical grade as solvent was purchased from Tianda Chemical Reagent Co. Ltd. (Tianjing, China) and dehydrated by adding CaH_2 and then distilled. Sulfuric acid (H_2SO_4) was purchased from Dongda Co. Ltd. (Henan, China), and used as-received.

2.2. Preparation of starch nanocrystals

According to the previous report [8], 36.725 g of potato starch granules was dispersed into 250 mL of 3.16 M H_2SO_4 aqueous solution, and then stirred for five days at 40 °C with a stirring speed of 100 rpm. Subsequently, the crude suspension containing starch nanocrystals (StNs) was centrifuged and then washed by distilled water repeatedly for more than five times until the pH approximately approached 7.0. At last, the StN precipitate was ultrasonically homogenized in an aqueous solution for 3 min using a JY92-2D ultrasonic instrument (Ningbo Scientz Biotechnology Co. Ltd., China) for the TEM observation and for the preparation of nanocomposites by Methods I and II. At the same time, a portion of the StN precipitate was lyophilized as loose powder for XRD measurement or then dispersed in butanone for the preparation of nanocomposites by Method III. TEM image of StNs is shown in Fig. 1. Although the StNs tended to self-aggregate, the distinguished isolated StNs were observed having the width of 10–20 nm and the length of 40–70 nm.

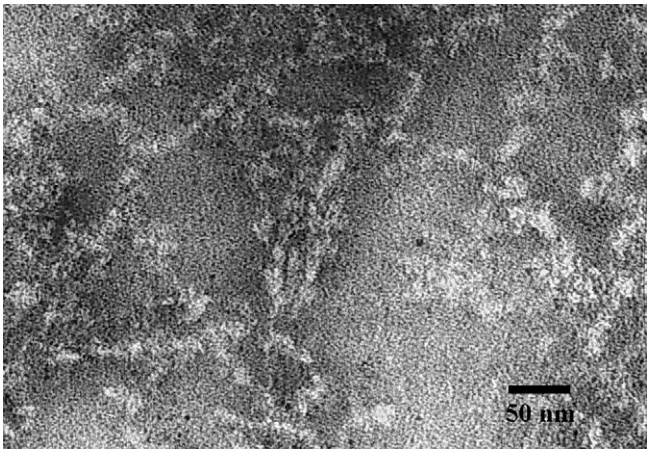

Fig. 1. TEM image of negatively stained potato starch nanocrystals.

2.3. Preparation of StN/WPU nanocomposites

The synthesis of waterborne polyurethane (WPU) is depicted as follows. Both 5.37 g PBA_{2000} and 1.87 g TDI (NCO/OH molar ratio = 4.0) were firstly placed into a three-necked round-bottomed flask equipped with a mechanical stirrer, a reflux condenser and an inlet of dry nitrogen. Subsequently, the reactant was heated up to ca. 70 °C, and then kept for mechanical stirring under a nitrogen atmosphere for 2 h. Thereafter, DMPA as chain-extender was dispersed into butanone and then added to give a NCO/OH molar ratio of 1.6. The reaction temperature was elevated up to 85 °C, followed by keeping up the reaction for 1 h. In this period, butanone was occasionally supplied in order to lower the viscidity of reactant. Afterward, the resultant product was cooled down to lower than 40 °C, and then neutralized −COOH of DMPA in polyurethane chains by adding TEA. At last, the emulsification was carried out by adding icy water under severe shearing to produce WPU latex with a solid content of 15 wt%. The WPU latex was caste on the Teflon mold after vacuum degassing, and then solidified as a film at 60 °C via evaporating water.

In such process of preparing the WPU film, the given weight of StNs were introduced at three stages, respectively, i.e. mixing with WPU latex post of emulsification (Method I), in the midst of emulsification (Method II) and chain-extending of polyurethane prepolymer (Method III), and finally produced the nanocomposite films of StNs filled WPU (US). When mixing with WPU latex (Method I) and in the midst of emulsification (Method II), the StN aqueous dispersion via ultrasonic treatment was used. As regards to introducing StNs at the stage of chain-extending (Method III), the dispersed StNs in butanone were added with DMPA. The US films prepared by Method I were coded as US-1, US-2, US-4, US-5 and US-8, where the numbers represent the theoretical content of StN in whole solid films. At the same time, the US nanocomposites containing 5 wt% StN prepared by Methods II and III were coded as US-5-II and US-5-III, respectively.

2.4. Characterization

ATR-FTIR spectra of all the films were recorded on an FTIR 5700 spectrometer (Nicolet, USA) using Smart OMNT reflect accessories in the range of 4000–700 cm^{-1}.

XRD patterns were recorded on D/Max-IIIA X-ray diffractor (Rigaku, Japan) using Cu Kα radiation (0.154 nm) at 40 kV and 60 mA with a scan rate of 12° min^{-1}. The diffraction angle of 2θ ranged from 2° to 60°.

TEM photographs of StNs were taken with an H-7000FA transmission electron microscope (Hitachi, Japan) at an acceleration voltage of 75 kV. Deposited StNs were negatively stained with an aqueous 2% solution of uranyl acetate before observation.

SEM observation was carried out on a JSM6700F scanning electron microscope (JEOL, Japan) with an accelerating voltage of 5 kV. The films were frozen in liquid nitrogen and then snapped immediately. The fracture surfaces were sputtered with Pt, and then observed and photographed.

DSC analysis was carried out on a DSC-204 instrument (Netzsch, Germany) under nitrogen atmosphere at a heating or cooling rate of 20 °C min^{-1}. The specimen was scanned in the range of −150 °C to 100 °C after a pretreatment of eliminating thermal history and removing volatile (heating from 20 °C to 100 °C and then cooling down to −150 °C).

DMA measurement was carried out on a DMA-242C dynamic mechanical analyzer (Netzsch, Germany) at a frequency of 1 Hz in the range from −150 °C to 100 °C with a heating rate of 3 °C min^{-1}. A dual cantilever device was used while the specimen size was 40 × 10 × ca. 0.5 mm^3.

The tensile strength (σ_b), elongation at break (ε_b) and Young's modulus (E) were measured on a CMT6503 universal testing machine (SANS, Shenzhen, China) with a crosshead rate of 200 mm min^{-1} according to GB13022-91. The tested specimens were cut into quadrate strips with a width of 10 mm while the distance between testing marks was 30 mm. An average value of five replicates of each sample was taken. During stressing, the specimens occurred with great elongation. So we regulated the data as follows: the nominal strain (ε_{nom}) and the nominal stress (σ_{nom}) were calculated by $\varepsilon_{nom} = e/L_0$ and $\sigma_{nom} = F/S_0$, respectively. Herein, S_0 and L_0 are, respectively, the initial area of cross-section and the initial marked length, while e and F are, respectively, the increment of length and the testing force. Subsequently, the true strain (ε_{true}) can be determined by $\varepsilon_{true} = \ln(L/L_0)$, where L is the actual length of the specimen before breaking ($L = L_0 + e$). The true stress (σ_{true}) can be calculated by $\sigma_{true} = F/S$, where S is the true area of cross-section after elongation. S was determined by assuming that the total volume of the specimen remained constant during testing, and so $S = S_0L_0/L$.

3. Results and discussion

3.1. Mechanical properties of nanocomposites

Fig. 2 shows the effect of the StN content on the mechanical properties of the US nanocomposites prepared by Method I, including tensile strength ($\sigma_{b,nom}$), elongation at break ($\varepsilon_{b,nom}$) and Young's modulus (E). Compared with $\sigma_{b,nom}$ of 11.0 MPa, $\varepsilon_{b,nom}$ of 814.4% and E of 2.7 MPa for neat WPU, it is worth noting that all the US nanocomposites showed the simultaneous enhancements in $\sigma_{b,nom}$, $\varepsilon_{b,nom}$ and E. With an increase of StN content, three mechanical parameters of the nanocomposite films increased simultaneously while the loading level is low. The $\varepsilon_{b,nom}$ reached a maximum value of 1406.6% when filling 2 wt% StNs, followed by a continuous decrease. At the same time, the $\sigma_{b,nom}$ and E increased up to 51.5 MPa and 5.2 MPa, respectively, until the StN loading reached 5 wt% and then both decreased. As a result, two US nanocomposites are highly recommended: (i) the US-2 containing only 2 wt% StNs had the maximum $\varepsilon_{b,nom}$ and enhanced $\sigma_{b,nom}$ as ca. 1.7- and 2.6-fold over those of WPU, respectively; (ii) the US-5 filled with 5 wt% StNs had the highest $\sigma_{b,nom}$, which were enhanced by ca. 370%, with slight increase of elongation unexpectedly.

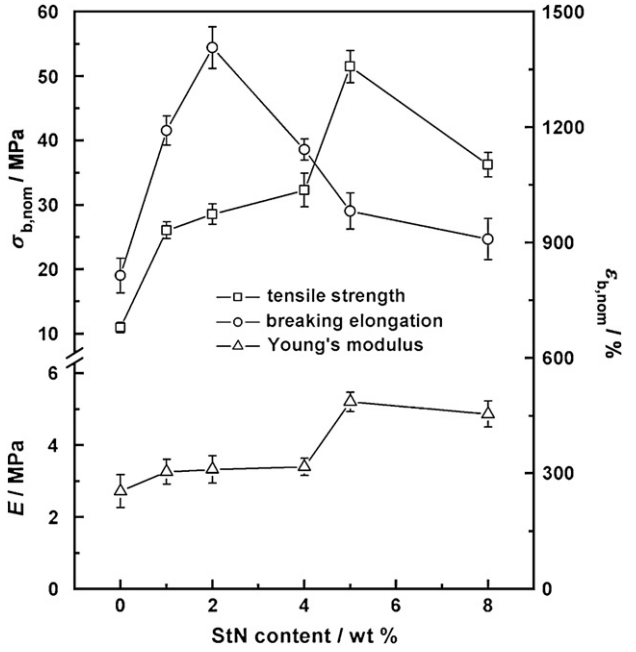

Fig. 2. Effects of the StN content on the tensile strength ($\sigma_{b,nom}$), elongation at break ($\varepsilon_{b,nom}$) and Young's modulus (E) of the US nanocomposites as well as the WPU reference.

Fig. 3 depicts the effects of chemical grafting on the US nanocomposites, which were prepared by adding 5 wt% StNs at three given stages in the process of synthesizing WPU, such as mixing with WPU latex post of emulsification (Method I), in the midst of emulsification (Method II) and chain-extending of polyurethane prepolymer (Method III). In such three stages, the numbers of active −NCO groups were distinctly different, resulting in the extent of chemical grafting between the StN surface and polyurethane chains in the order of Method I < II < III. Obviously, the $\sigma_{b,nom}$ and $\varepsilon_{b,nom}$ decreased with an increase of chemical grafting. However, the US-5-III with highest chemical grafting had the maximum E (24.03 MPa) in spite that the US-5-II with moderate chemical grafting showed lower E value than the US-5, in which only physical interaction occurred between StN nano-filler and WPU matrix. However, although chemical grafting inhibited mechanical performances, three mechanical parameters of US-5-II and US-5-III were still higher than those of neat WPU.

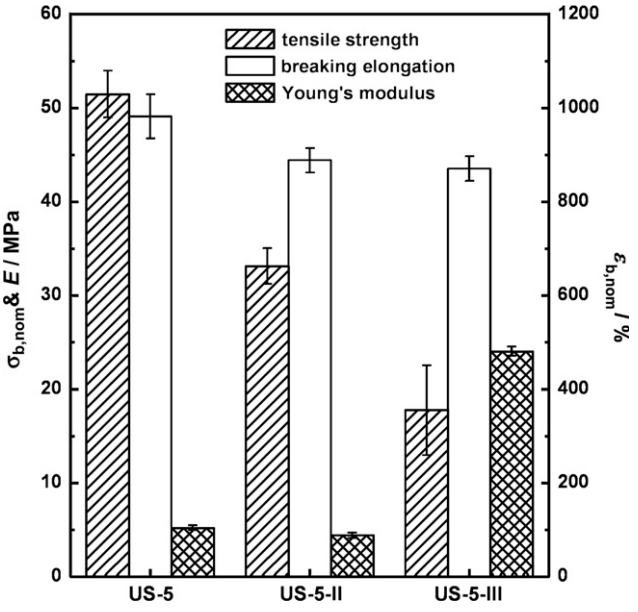

Fig. 3. Effects of the compounding method on the tensile strength ($\sigma_{b,nom}$), elongation at break ($\varepsilon_{b,nom}$) and Young's modulus (E) of the US nanocomposites containing 5 wt% StNs.

In view that the US nanocomposites can endure great strain, the true values of tensile strength and elongation at break ($\sigma_{b,true}$ and $\varepsilon_{b,true}$), which are summarized in Table S1, might represent the practical performances in service. It is worth noting that the US-2 with highest elongation had higher $\sigma_{b,true}$ (430.3 MPa) than US-4 (401.1 MPa) in spite that the US-4 had higher $\sigma_{b,nom}$. For US-5, the $\sigma_{b,true}$ reached 556.9 MPa as ca. 5.6-fold over that of WPU.

The simultaneous enhancements in strength, elongation and Young's modulus might be attributed to the uniform dispersion of StNs in nano-scale [44] as well as the physical interaction and chemical grafting between StN nano-filler and WPU matrix. The strong interfacial interaction confirmed the transferring of the stress burdened by WPU matrix to the rigid StN nano-filler. However, with an increase of the loading level of StNs, the self-aggregation of StNs might break the original structure and interaction in WPU matrix, and even cause severe microphase separation between StN nano-phase and WPU matrix. It decreased mechanical performances, and especially for elongation. In addition, chemical grafting partly hindered the formation of physical interaction due to steric exclusion of covalent bonds, resulting in a decrease of strength and elongation.

3.2. Hydrogen bonding in nanocomposites

As well known, hydrogen bonds are a kind of essential physical interaction in waterborne polyurethane, which nearly affects microphase separation structure between hard- and soft-segments and mechanical properties of materials. In this case, the −NH in hard-segment is hydrogen-bonded with the urethane −C═O of hard-segments and the ester −C═O of the PBA_{2000} soft-segments. In addition, −OH on the StN surface also participated in hydrogen bonding with −C═O in the soft- and hard-segments. Fig. 4 shows the ATR-FTIR spectra of the US nanocomposites containing various StN contents as well as the WPU reference (A) and the US nanocomposites with 5 wt% StN prepared by three methods (B). Herein, the −NH bands of WPU consisted of a main peak located at ca. 3342 cm^{-1} with a shoulder peak located at ca. 3516 cm^{-1}. All the US nanocomposites showed the analogical −NH bands in spite that the absorption of −OH in StNs was embedded in those. As a result, the absorptions above 3000 cm^{-1} of all the US nanocomposites and WPU were divided into two peaks by curve-fitting (Fig. S1), i.e. Peak I located at 3518–3522 cm^{-1} and Peak II located at 3320–3325 cm^{-1}. The former was the

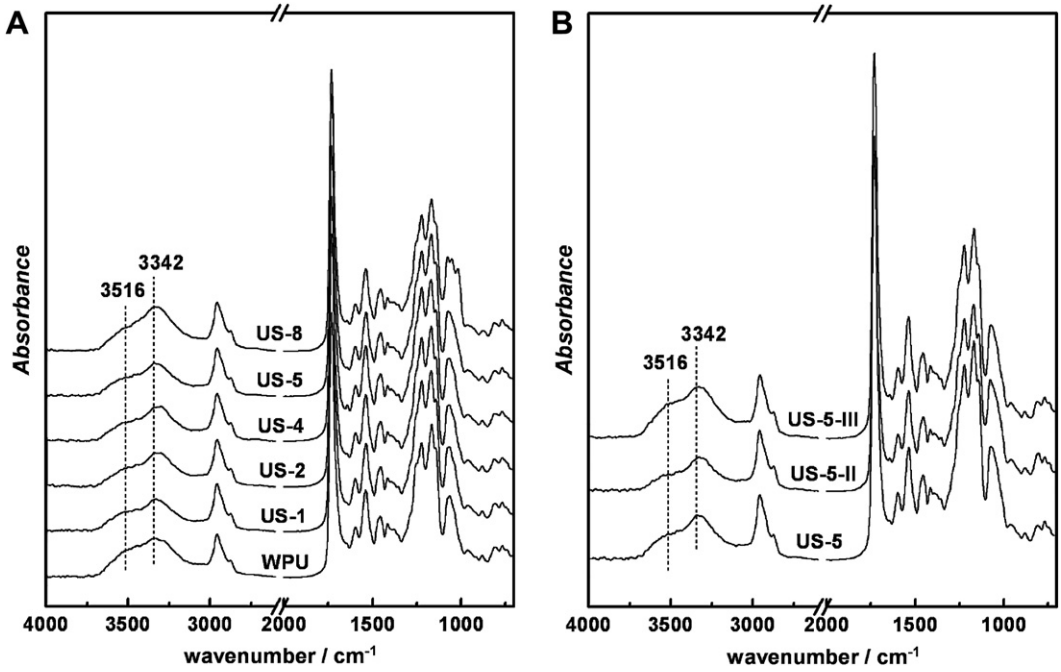

Fig. 4. ATR-FTIR spectra of the US nanocomposites and the WPU reference. ((A): the US nanocomposites with various StN contents; (B): the US nanocomposites containing 5 wt% StNs prepared by three methods.)

free −NH absorption while the latter was the absorption of hydrogen-bonded −NH for WPU or included the additional −OH absorption for the US nanocomposites. Table 1 summarizes the detailed location and fraction of Peaks I and II for all the US nanocomposites and WPU. With an increase of StN content, the percentage of −OH number in StN vs. all the −OH and −NH in the nanocomposites increased from ca. 7.1% (adding 1 wt% StNs) to ca. 37.1% (adding 8 wt% StNs). Apparently, the increasing fraction of Peak II was not proportional to the increment contributed by −OH absorption. It indicated that the original hydrogen bonds associated with −NH in WPU matrix were cleaved. When the StN loading was lower than 2 wt%, the relatively prominent increase of fraction for Peak II was attributed to less extent of breaking −NH-based hydrogen bonds and the formation of hydrogen bonds associated with −OH on the StN surface. In addition, with an increase of chemical grafting, the fraction of Peak II increased for the US nanocomposites containing the same loading level of 5 wt% StNs prepared by three methods, indicating that chemical grafting hindered the cleavage of original hydrogen bonds associated with −NH in WPU matrix.

The analogical −C═O bands of the US nanocomposites and WPU were also divided into three peaks (Fig. S2), namely the Peak III of free −C═O located at 1733−1734 cm^{-1}, the Peak IV of hydrogen-bonded −C═O in amorphous region located at 1716−1718 cm^{-1} and the Peak V of hydrogen-bonded −C═O in ordered domain located at 1697−1699 cm^{-1} [45]. The location and fraction of such three peaks for the US nanocomposites and WPU are also summarized in Table 1. Obviously, adding StNs slightly decreased the fraction in free −C═O peak (Peak III), indicating that the hydrogen bonding associated with −C═O of hard-segments and PBA_{2000} soft-segments was improved. It was attributed to newly forming hydrogen bonds between −C═O of WPU

Table 1
Location and fraction of curve-fitting peaks for the −NH and −C═O bands in the FTIR spectra of the US nanocomposites and WPU

Sample code	−NH band				−C═O band					
	Peak I		Peak II		Peak III		Peak IV		Peak V	
	Location/cm^{-1}	Fraction/%	Location/cm^{-1}	Fraction/%	Location/cm^{-1}	Fraction/%	Location/cm^{-1}	Fraction/%	Location/cm^{-1}	Fraction/%
WPU	3520.0	35.6	3320.8	64.4	1733.1	64.8	1717.3	23.1	1697.2	12.1
US-1	3520.0	32.1	3324.0	67.9	1733.5	61.4	1717.0	27.2	1698.3	11.4
US-2	3518.9	23.1	3320.7	76.9	1733.5	62.6	1717.3	25.7	1697.2	11.7
US-4	3518.9	34.8	3320.7	65.2	1733.3	63.3	1717.0	25.3	1697.2	11.4
US-5	3520.0	37.9	3322.9	62.1	1733.3	64.1	1716.8	25.6	1697.7	10.3
US-8	3518.9	30.5	3323.0	69.5	1733.5	62.5	1716.6	27.7	1697.7	9.8
US-5-II	3521.2	33.2	3321.8	66.8	1733.9	62.7	1717.3	26.7	1697.5	10.7
US-5-III	3520.0	32.2	3324.1	67.8	1733.5	61.8	1716.6	27.0	1698.3	11.2

Peak I: free −NH; Peak II: hydrogen-bonded −NH for WPU, and hydrogen-bonded −NH and −OH in StNs for the US nanocomposites; Peak III: free −C═O; Peak IV: hydrogen-bonded −C═O in amorphous region; Peak V: hydrogen-bonded −C═O in ordered domain.

component and −OH on the StN surface. With an increase of StN content, the fraction of free −C═O firstly increased until 5 wt% StN, and then decreased for US-8. The initial increase of free −C═O fraction resulted from the cleavage of original hydrogen bonds in WPU matrix. A second decrease of free −C═O fraction for US-8 might be attributed to the preserving of original hydrogen bonds between soft- and hard-segments because the size expansion of StN nano-phase increased the extent of microphase separation between StN and WPU matrix. In addition, with an increase of chemical grafting, the fraction of free −C═O gradually decreased. It was in agreement with the analysis on −NH bands, namely chemical grafting inhibited the formation of hydrogen bonds on the StN surface and then facilitated keeping up the original hydrogen bonds in WPU matrix. Although hydrogen bonding associated −C═O was improved on the whole, the effect of adding StN on the region of hydrogen bonding in the nanocomposites was distinctly different. The increasing fraction of Peak IV suggested that the improvement of hydrogen bonding mainly happened in amorphous region, while the slight decreasing fraction of Peak V proved the cleavage of hydrogen bonding in ordered domain. Usually, the hydrogen bonding in ordered domain was constructed by the hard-segments in WPU matrix. As a result, adding StN pulled down the original ordered alignment among hard-segments, and so the extent of breakage increased with an increase of StN content, shown as a continuous decrease of Peak V fraction. On the other hand, considering the cleavage of hydrogen bonds associated with −NH mentioned above, increasing fraction of Peak IV was attributed to the formation of hydrogen bonds between −OH on the StN surface and −C═O. It indicated that the StNs might mainly disperse into the amorphous region of WPU matrix. With an increase of chemical grafting, the fractions of hydrogen-bonded −C═O in amorphous region and ordered domain simultaneously increased. In view of the increase of fraction of hydrogen-bonded −NH mentioned above, the increasing fractions of Peaks IV and V for the US-5-II and US-5-III were mainly attributed to hydrogen bonding between −NH and −C═O in WPU matrix.

3.3. Amorphous nature of nanocomposites and crystalline state of StN

Fig. 5 shows the XRD patterns of the US nanocomposites with various StN contents prepared by Method I and containing 5 wt% StN prepared by Methods II and III as well as WPU and StNs. All the US nanocomposites inherited amorphous nature of neat WPU, shown as a diffuse peak located at 20.28° of 2θ, in spite that −C═O-based hydrogen bonds constructed a small scale of ordered domains in WPU matrix as mentioned above. Although the StNs showed a semi-crystalline character with two well-defined diffraction peaks located at 17.06° and 22.3° of 2θ, they were absent in nanocomposites because of low loading level (lower than 5 wt%) and relatively uniform dispersion. However, when the StN content increased up to 8 wt%, a shoulder peak appeared at 17.6° of 2θ, which corresponded to the strongest diffraction of semi-crystalline StNs. It proved that the StNs in nanocomposites tended to self-aggregate with an increase of StN content.

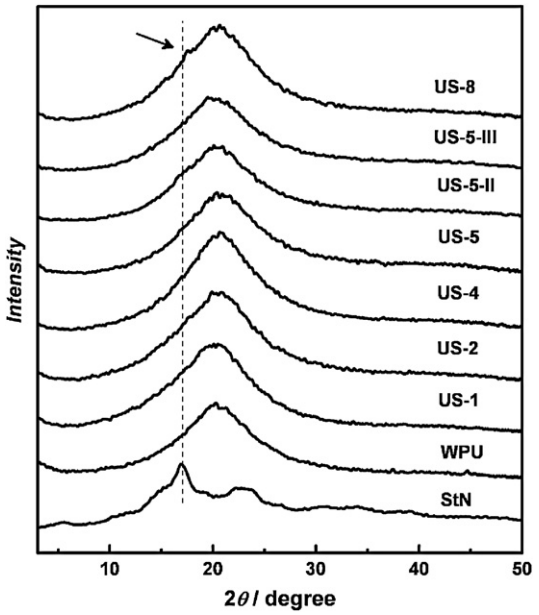

Fig. 5. XRD patterns of the US nanocomposites as well as the WPU reference and the freeze-dried StN powder.

3.4. Thermal behavior of nanocomposites

DSC and DMA were used to further understand the interaction between StN nano-filler and WPU matrix as well as the structural changes of WPU matrix and the distribution of StNs, by observing the variances of domain-scale glass transition and molecular-level α-relaxation assigned to the PBA_{2000} soft-segment, respectively. Table 2 summarizes the glass transition temperature at midpoint ($T_{g,mid}$) and heat-capacity increment (ΔC_p) from DSC thermograms (Fig. 6). In the US nanocomposites, the temperatures of glass transition (T_g) and α-relaxation (T_α) of the PBA_{2000} soft-segment can be affected by StNs in two opposite ways. First, the motion of soft-segment might be suppressed by rigid StN nano-phase mediated by hydrogen bonding or chemical grafting onto active StN surface. It could result in the shift of T_g and T_α to high temperature. In the opposite way, incorporating StNs might cleave the original interaction between hard- and soft-segments and hence change the microphase structure in WPU matrix. For example, the soft-segment can escape from the binding of hard-segment to give decreasing T_g and T_α. Obviously, the $T_{g,mid}$s of all the US nanocomposites were higher than that of WPU, suggesting that the restriction of StNs to the mobility of soft-segments was dominant in spite of the inevitable cleavage of the original interaction between hard- and soft-segments in WPU matrix. When the StN content was less than 2 wt%, the rigid StNs could homogeneously dissolve into the WPU matrix, and then inhibit the motion of soft-segment mediated with newly formed interaction with WPU component. At this time, the $T_{g,mid}$s increased with an increase of StN content. However, when the StN content ranged from

Table 2
DSC and DMA data of the US nanocomposites and WPU as reference

Sample code	DSC data for glass transition		DMA data for α-relaxation				
			log E'–T curves			tan δ–T curves	
	$T_{g,mid}$/°C	ΔC_p/J g^{-1} K^{-1}	$T_{\alpha,onset}$/°C	log $E'_{T\alpha}$/MPa	log $E'_{T\alpha+30}$/MPa	$T_{\alpha,max}$/°C	$H_{loss\text{-}peak}$
WPU	−41.3	0.412	−49.1	3.90	3.50	−37.1	0.263
US-1	−41.0	0.384	−47.1	3.78	3.50	−36.5	0.223
US-2	−40.1	0.361	−46.4	3.87	3.47	−35.9	0.244
US-4	−40.6	0.391	−48.8	3.25	2.82	−36.9	0.262
US-5	−41.0	0.355	−46.0	3.10	2.80	−35.4	0.239
US-8	−40.5	0.362	−46.5	3.90	3.55	−36.5	0.232
US-5-II	−39.8	0.338	−45.9	3.05	2.45	−35.1	0.254
US-5-III	−40.3	0.381	−44.9	3.17	2.65	−34.1	0.267

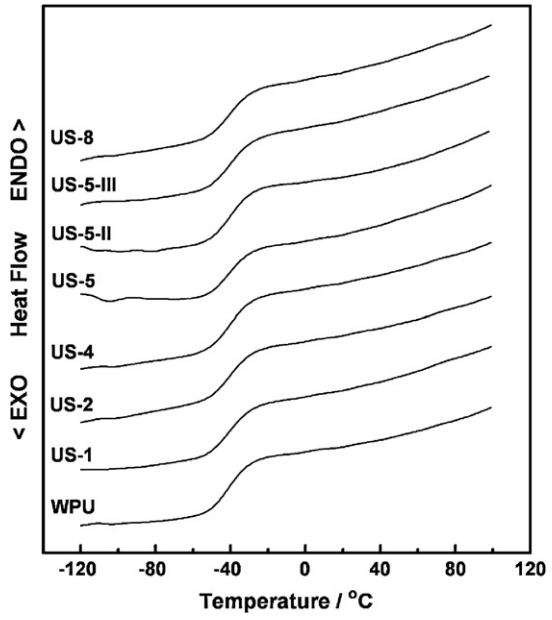

Fig. 6. DSC thermograms of the US nanocomposites and the WPU reference.

2 wt% to 5 wt%, the $T_{g,mid}$s gradually decreased instead because increasing StN content induced the self-aggregation of StNs and hence weakened the restriction to the motion of soft-segment. Thereafter, excess great StN aggregates in US-8 containing 8 wt% StNs, proved by a shoulder peak in XRD pattern, might increase the extent of microphase separation between StN nano-phase and WPU matrix. The preserving of original interaction between soft- and hard-segments gave an increasing $T_{g,mid}$ for US-8. In addition, no endothermic peak, assigned to ordered aggregation of hard-segments, is observed in all the DCS thermograms, verifying amorphous nature of all the US nanocomposites and WPU. This is in good agreement with the XRD result.

DMA is a powerful technique to reflect the mobility of soft-segment through α-relaxation at molecular-level, for which the specific heat increment of glass transition at domain-scale measured from DSC is generally ill-defined. DMA curves of all the US nanocomposites and WPU are depicted in Figs. 7 and 8, while Table 2 summarizes the α-relaxation temperature ($T_{\alpha,max}$) and height of loss-peak ($H_{loss\text{-}peak}$) from tan δ–T curves as well as α-relaxation temperature at onset ($T_{\alpha,onset}$) and storage modulus at onset temperature (log $E'_{T\alpha}$) and at $T_{\alpha,onset}+30$ °C (log $E'_{T\alpha+30}$) from log E'–T curves (Figs. 7 and 8). In the tan δ–T curves, the shift of $T_{\alpha,max}$s to higher temperatures for the nanocomposites as well as the reduced magnitude of loss-peak suggested that the energy dissipation process is slowed down by the nano-fillers. It means that the interactions between the soft-segments in WPU matrix and the StN nano-fillers are stronger and therefore the mobility of soft-segment decreased [46]. In this case, the suppression of StNs to soft-segments was proportional to the effective surface of StNs. When the StNs homogeneously dissolved into WPU matrix (the StN content < 2 wt%), the increasing interfacial area between StN nano-filler and WPU matrix resulted in the increase of $T_{\alpha,max}$s and $T_{\alpha,onset}$s with an increase of StN content. It is in good agreement with the DSC results. Thereafter, with a continual increase of StN content, the StNs gradually self-aggregated. Although the self-aggregation of StNs induced the expansion of size, the number of StN nano-phase necessarily increased at one time. As a result, the $T_{\alpha,max}$ and $T_{\alpha,onset}$ of US-5 increased once more after an obvious decrease for US-4. At last, excess great StN nano-phase severely decreased the effective interface for producing the interaction between StN nano-filler and WPU matrix. The US-8 gave decreasing $T_{\alpha,max}$ and $T_{\alpha,onset}$. It was worth noting that adding 5 wt% StNs gave the highest $T_{\alpha,max}$ and $T_{\alpha,onset}$, but the lowest $T_{g,mid}$ from DSC in all the US nanocomposites. It suggested that the unbinding of soft-segments from hard-segments at domain-scale contributed to the lowest $T_{g,mid}$, in spite that the strong interaction happened on the StN surface at molecular-level highly restricted the motion of soft-segments and gave the highest $T_{\alpha,max}$ and $T_{\alpha,onset}$. In the US nanocomposites, the rigidity was contributed by the nano-phase of StNs [47] except for the hard-segment domain in WPU matrix. Thus, the log $E'_{T\alpha}$s of the US nanocomposites with the StN content lower than 5 wt%, which represent the rigidity of glassy state, decreased in contrast with the increase of $T_{\alpha,onset}$. It was attributed to the cleavage of ordered hard-segment domains, which was proved by the FTIR results, in spite of the improving stiffness of the StN nano-phase. However, when the StN loading was 8 wt%, the preserving of the structure for WPU matrix as well as the increasing greater phase of aggregated StNs gave a log $E'_{T\alpha}$ value of US-8 close to that of neat WPU. Usually, the Young's modulus (E) of the material

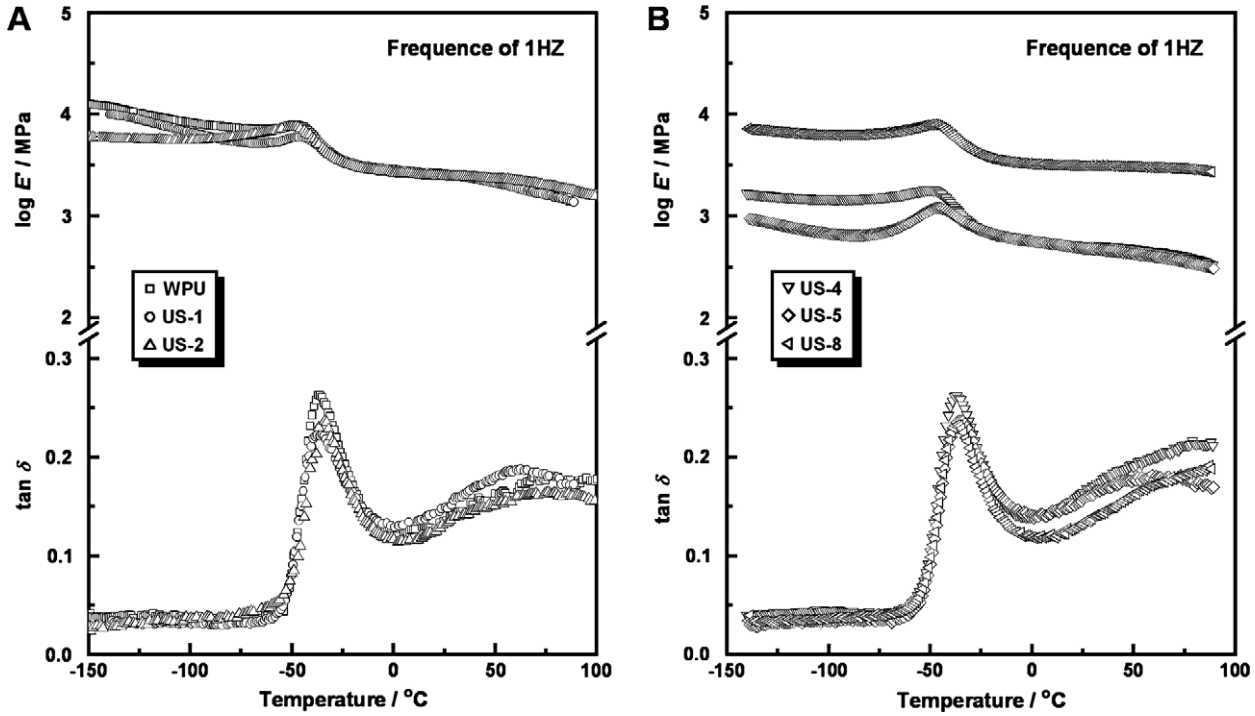

Fig. 7. Logarithm of storage modulus (log E') and tangent of loss angle (tan δ) vs. temperature measured at 1 Hz for the US nanocomposites with various StN contents and the WPU reference.

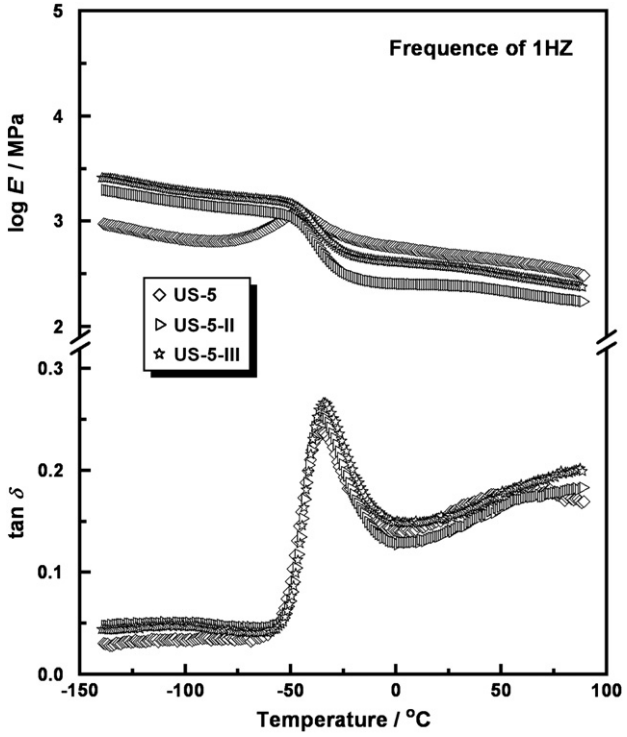

Fig. 8. Logarithm of storage modulus (log E') and tangent of loss angle (tan δ) vs. temperature measured at 1 Hz for the US nanocomposites containing 5 wt% StNs prepared by three methods.

is in positive correlation with the log $E'_{T\alpha+30}$. However, it is interesting that the variance of log $E'_{T\alpha+30}$ functioned as the StN content was just opposite to that of E measured by tensile test. It indicated that the reinforcing role of StN immersed into the soft-segments was dominant in spite that the cleavage of hard-segment domain decreased the rigidity of WPU matrix. However, the higher log $E'_{T\alpha+30}$ of US-8, in contrast with that of neat WPU, resulted from the preserving of the structure of WPU matrix.

When applying Methods II and III to produce covalent bonding between StNs and WPU components, chemical grafting distinctly resulted in the shift of $T_{g,mid}$s, $T_{\alpha,max}$s and $T_{\alpha,onset}$s to high temperature. FTIR results pointed out that chemical grafting facilitated keeping up the original interaction between soft- and hard-segments in WPU matrix. As a result, although the steric hindrance of chemical grafting inevitably interfered with the formation of physical interaction between StN nanofiller and WPU matrix, the synergistic effect of the formed covalent bonds on the StN surface and the binding of hard-segments contributed to increasing $T_{g,mid}$s, $T_{\alpha,max}$s and $T_{\alpha,onset}$s of US-5-II and US-5-III. With an increase of chemical grafting, DMA results showed a continuous increase of $T_{\alpha,max}$s and $T_{\alpha,onset}$s, but DSC results showed that the $T_{g,mid}$s firstly increased for US-5-II followed by a decrease for US-5-III. It indicated that the increase of chemical grafting obviously augmented the restriction of soft-segment motion at molecular-level. However, on domain-scale reflected by DSC, the highest $T_{g,mid}$ of US-5-II was attributed to the cooperative effect of three factors, namely the interaction between soft- and hard-segments must be considered except for the extent of physical interaction and chemical grafting between StN and WPU. The variances of log $E'_{T\alpha}$ and log $E'_{T\alpha+30}$ functioned as the extent of chemical grafting were same as those of E. However, although the chemical grafting facilitated preserving the original interaction of WPU matrix, the log $E'_{T\alpha}$ and

log $E'_{T\alpha+30}$ values of the US nanocomposites containing chemical grafting were lower than those of the physically blended US-5. It was due to the expense of −NCO groups in the process of chemical grafting, which is essential to form the hard-segments.

3.5. Fractured morphology of nanocomposites

Fig. 9 shows the SEM images of fractured surfaces for the US nanocomposite and WPU. When the StN content was lower than 2 wt%, the US nanocomposites (Fig. 9B and C) showed the fractured surface of fluctuant morphology similar to WPU (Fig. 9A). It suggested that a small amount of StNs homogeneously dispersed into WPU matrix with a small size and almost did not change the original structure and fractured behavior of WPU. However, with a continuous increase of StN loading (higher than 4 wt%), the fractured surface gradually became smooth with densely fluctuant thin stripes. It was attributed to the breakage of original structure in WPU matrix after adding higher loading level of StNs. In addition, with an increase of chemical grafting, the fractured surface of US-5-II and US-5-III also gradually became smoother, showing a relative brittle character. It was in agreement with the decrease of strength and elongation at break. Apparently, SEM images declared the effects of the increasing number and expanded size of StN nano-phase with the elevating StN loading level as well as the effects of chemical grafting extent on the greater-scale structure in the nanocomposites.

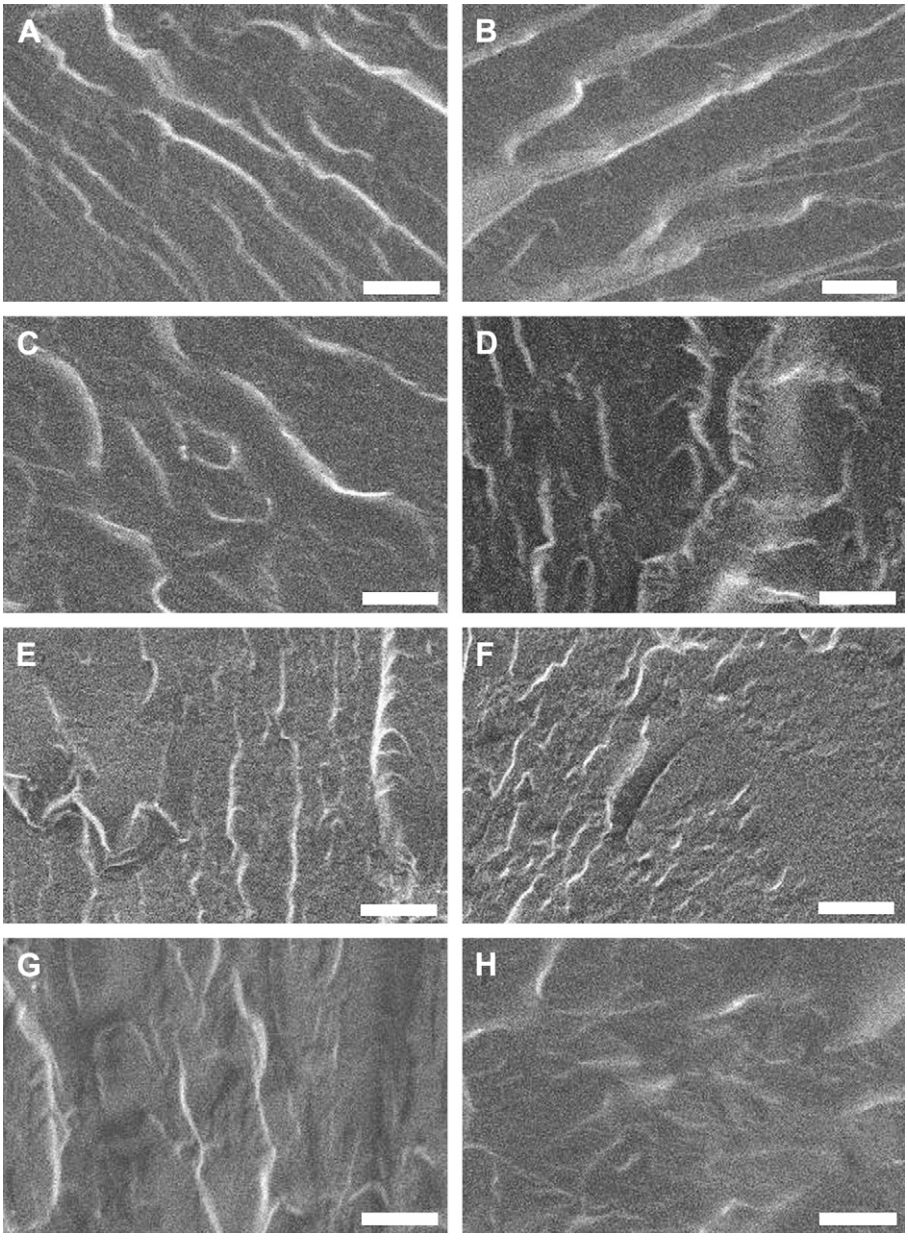

Fig. 9. SEM images of fractured surface of the US nanocomposites with various StN contents prepared by different methods and the WPU reference. ((A): WPU; (B): US-1; (C): US-2; (D): US-4; (E): US-5; (F): US-8; (G): US-5-II; (H): US-5-III.) The scale of all the bars in the images is 10 μm.

3.6. Mechanism of simultaneous reinforcing and toughening

Low loading level (lower than 2 wt%) induced the uniform dispersion of StNs, resulting in less cleavage of original structure and interaction in WPU matrix and the forming of strong physical interaction on the StN surface. It was worth noting that the US-2 had the highest elongation, which was ca. 1.7-fold over that of WPU, with enhanced strength and Young's modulus. With an increase of StN content, the size of StN nano-phase inevitably expanded due to the strong self-aggregation tendency of StNs while the number of nano-phase augmented at one time. It not only decreased the effective active surface of StNs, but also increased the breakage of the original structure and interaction in WPU matrix and even induced microphase separation between StN nano-phase and WPU matrix. As a result, after US-5 reached the maximum strength and Young's modulus, all the mechanical parameters decreased with a continuous increase of StN content because of the formation of such big StN agglomerates [48]. Meanwhile, the decrease of elongation was prior to strength and Young's modulus, and happened when the StN content was higher than 2 wt%. The simultaneous enhancements in strength, Young's modulus and elongation were mainly attributed to enduring stress of rigid StN and the stress transferring mediated with strong interaction between StN surface and WPU matrix as well as the relative uniform dispersion of the StN nano-filler [44]. At the same time, the excess breakage of original structure and interaction in WPU matrix as well as the microphase separation between StN nano-filler and WPU matrix inhibited further enhancement of mechanical performances. Unexpectedly, the chemical grafting between StN surface and WPU component cannot give higher strength. In view of the inhibition of chemical grafting to forming physical interactions on StN surface, the synergistic effect of physical interaction might facilitate stress transferring much more, which is the key factor for enhancing mechanical performances. In addition, the increase of network density, contributed by chemical grafting, decreased the elongation.

4. Conclusions

New nanocomposite materials were prepared by casting and evaporating the mixture of waterborne polyurethane (matrix) and starch nanocrystals (nano-filler). Moreover, the strength, elongation and Young's modulus were simultaneously enhanced. Herein, two US nanocomposites were worth noting: (i) the US-2 containing only 2 wt% StNs had the maximum elongation (1406.6%) and enhanced tensile strength (28.6 MPa) as ca. 1.7- and 2.6-fold over those of neat WPU, respectively; (ii) the US-5 filled with 5 wt% StNs had the highest tensile strength (51.5 MPa) and increased Young's modulus (5.2 MPa), which were enhanced by ca. 370% and ca. 93%, respectively, with an increasing elongation (981.9%). The prominent improvement of mechanical performances, i.e. simultaneous reinforcing and toughening, was attributed to enduring stress of rigid StN and stress transferring mediated with strong interaction on the interface between StN nano-filler and WPU matrix. Meanwhile, the preserving of original structure and interaction in WPU matrix was still a second crucial factor for further enhancing the mechanical performances. Furthermore, chemical grafting was verified not to be in favor of enhancing strength and elongation due to inhibiting the formation of physical interaction on the StN surface and increasing the network density of nanocomposites.

Different from the other reports of filling high content of whisker and nanocrystal into polymer matrix to simply increase strength and modulus, we realized the simultaneous reinforcing and toughening for waterborne polyurethane-based nanocomposites using low loading level (less than 8 wt%) of rigid nanoparticle, such as starch nanocrystals. Such new green bionanocomposite materials with superior mechanical properties could be believed to have great potential applications.

Acknowledgements

Financial support from State Key Laboratory of Polymer Physics and Chemistry (Changchun Institute of Applied Chemistry, Chinese Academy of Sciences), and Canadian Biomass Innovation Network (CBIN) project TID 824.

Appendix. Supplementary data

Supplementary data associated with this article can be found, in the online version, at doi:10.1016/j.polymer.2008.02.020.

References

[1] Mecking S. Angew Chem Int Ed Engl 2004;43:1078.
[2] Smith R. Biodegradable polymers for industrial applications. CRC Press; 2005.
[3] Wool R, Sun XS. Bio-based polymers and composites. Elsevier Inc.; 2005.
[4] Darder M, Aranda P, Ruiz-Hitzky E. Adv Mater 2007;19:1309.
[5] Azizi Samir MAS, Alloin F, Dufresne A. Biomacromolecules 2005; 6:612.
[6] Paillet M, Dufresne A. Macromolecules 2001;34:6527.
[7] Putaux J-L, Molina-Boisseau S, Momaur T, Dufresne A. Biomacromolecules 2003;4:1198.
[8] Angellier H, Choisnard L, Molina-Boisseau S, Ozil P, Dufresne A. Biomacromolecules 2004;5:1545.
[9] Angellier H, Molina-Boisseau S, Dole P, Dufresne A. Biomacromolecules 2006;7:531.
[10] Angellier H, Molina-Boisseau S, Dufresne A. Macromolecules 2005;38: 9161.
[11] Yuan H, Nishiyama Y, Wada M, Kuga S. Biomacromolecules 2006;7: 696.
[12] Angellier H, Molina-Boisseau S, Belgacem MN, Dufresne A. Langmuir 2005;21:2425.
[13] Thielemans W, Belgacem MN, Dufresne A. Langmuir 2006;22:4904.
[14] Labet M, Thielemans W, Dufresne A. Biomacromolecules 2007;8:2916.
[15] Gopalan Nair K, Dufresne A. Biomacromolecules 2006;4:666.
[16] Ljungberg N, Cavaillé JY, Heux L. Polymer 2006;47:6285.
[17] Ljungberg N, Bonini C, Bortolussi F, Boisson C, Heux L, Cavaillé JY. Biomacromolecules 2005;6:2732.

[18] Chazeau L, Cavaillé JY, Canova G, Dendievel R, Boutherin B. J Appl Polym Sci 1999;71:1797.
[19] Garcia de Rodriguez NL, Thielemans W, Dufresne A. Cellulose 2006;13:261.
[20] Chauve G, Heux L, Arouini R, Mazeau K. Biomacromolecules 2005; 6:2025.
[21] Helbert W, Cavaillé JY, Dufresne A. Polym Compos 1996;17:604.
[22] Matos Ruiz M, Cavaillé JY, Dufresne A, Graillat C, Gerard JF. Macromol Symp 2001;169:211.
[23] Matos Ruiz M, Cavaillé JY, Dufresne A, Gerard JF, Graillat C. Compos Interfaces 2000;7:117.
[24] Cavaillé JY, Dufresne A, Paillet M, Azizi Samir MAS, Alloin F, Sanchez JY. French Patent FR2841255, 2002.
[25] Cao X, Dong H, Li CM. Biomacromolecules 2007;8:899.
[26] Dufresne A, Kellerhals MB, Witholt B. Macromolecules 1999;32:7396.
[27] Dufresne A. Compos Interfaces 2003;10:369.
[28] Kvien I, Tanem BS, Oksman K. Biomacromolecules 2005;6:3160.
[29] Petersson L, Kvien I, Oksman K. Compos Sci Technol 2007;67:2535.
[30] Morin A, Dufresne A. Macromolecules 2002;35:2190.
[31] Noshiki Y, Nishiyama Y, Wada M, Kuga S, Magoshi J. J Appl Polym Sci 2002;86:3425.
[32] Lu Y, Weng L, Cao X. Carbohydr Polym 2006;63:198.
[33] Angles MN, Dufresne A. Macromolecules 2001;34:2921.
[34] Lu Y, Weng L, Zhang L. Biomacromolecules 2004;5:1046.
[35] Wang Y, Cao X, Zhang L. Macromol Biosci 2006;6:524.
[36] Zheng H, Ai F, Chang PR, Huang J, Dufresne A. Polym Compos, in press.
[37] Wicks ZW, Wicks DA, Rosthauser JW. Prog Org Coat 2002;44:161.
[38] Noble KL. Prog Org Coat 1997;32:131.
[39] Wu Q, Zhang L. J Appl Polym Sci 2001;79:2006.
[40] Wang N, Zhang L. Polym Int 2005;54:233.
[41] Cui G, Xia W, Chen G, Wei M, Huang J. J Appl Polym Sci 2007;106: 4257.
[42] Jiang L, Zhang J, Wolcott MP. Polymer 2007;48:7632.
[43] Yu Z, Yin J, Yan S, Xie Y, Ma J, Chen X. Polymer 2007;48:6439.
[44] Kim DH, Fasulo PD, Rodgers WR, Paul DR. Polymer 2007;48:5960.
[45] Huang J, Zhang L. Polymer 2002;43:2287.
[46] Chausson S, Caignaert V, Retous R, Rueff J-M, Pluart LL, Madec P-J, et al. Polymer 2008;49:488.
[47] Cui L, Ma X, Paul DR. Polymer 2007;48:6325.
[48] Nguyen QT, Baird DG. Polymer 2007;48:6923.